Bull. Chem. Soc. Ethiop. **2024**, 38(1), 255-267.
DOI: https://dx.doi.org/10.4314/bcse.v38i1.19

ISSN 1011-3924
Printed in Ethiopia
Online ISSN 1726-801X

KINETICS, ISOTHERMS, AND THERMODYNAMIC MODELING OF LIGHT LANTHANIDES(III): La(III) AND Gd(III) USING Mn–Ni NANOPARTICLES

Y.F. El-Aryan*

Chemistry Department, College of Science, University of Bisha, Bisha 61922, Saudi Arabia

(Received August 15, 2023; Revised October 31, 2023; Accepted October 31, 2023)

ABSTRACT. The sorption of light lanthanides, La(III) and Gd(III) on Mn–Ni nanoparticle was studied at varying ions concentrations, pH, contact time and temperatures. The kinetics of sorption of La(III) and Gd(III) were investigated, the experimental data were analyzed using the pseudo-first-order, pseudo-second-order forms, Elovich, and intra-particle diffusion models. The sorption kinetics of investigated ions was described by pseudo-second-order model. The experimental isotherms data were analyzed using Freundlich, Langmuir, and Temkin models were used to analyze the sorption isotherm data of ion exchange of La(III) and Gd(III) on Mn–Ni nanoparticle. The best fit was obtained by the Langmuir model with high correlation coefficients ($R^2 = 0.995$) with a maximum monolayer adsorption capacity of 8.81 mg/g.

KEY WORDS: Sorption isotherm, Kinetics models, Mn–Ni nano particle

INTRODUCTION

Rare-earth elements (REE) have technical importance due to their wide application in different areas [1, 2] as these elements are named "The Vitamins of Modern Industry" [3]. They are used for electronic purposes, metallurgy, medical science, and optical technology. Gadolinium is a rare earth metal that has similar properties as other rare earth metals, making it difficult to separate Gadolinium from the others. Gadolinium has been extracted from Earth's crust in the form of their minerals, such as monazite and gadolinite. Gadolinium is widely used for applications in various fields, including medicine and chemical industries, and thus its concentration in the environment is important to note [4, 5]. La(III) is one of the most abundant rare earth elements. Rare earth elements are extensively used in metallurgy, lasers, textiles, petroleum agriculture, magnets, and batteries. A Swedish chemist Carl Gustav Mosander discovered La(III) in 1839, but in 1923, it was isolated in the pure form. Rare earths were originally used to designate the lanthanides which includes oxides of scandium, yttrium, lanthanum and 14 elements following lanthanum in the 3rd row of the periodic table, i.e. from cerium to lutetium [6]. The demand for REE has grown rapidly over the years, more than its supply rate. Many techniques are used for the recovery of REE to overcome this problem, such as ion exchange [7], co-precipitation [8], membrane [9], solvent extraction [10], electrochemical [11] and adsorption [11]. Desorption techniques are widely used due to their fast, easy operation and low cost. The efficiency of the adsorption process depends on the accessibility of the adsorbent. The main objective of the present work is directed to study the sorption of La(III) and Gd(III) from waste solution using strongly cationic exchange Mn–Ni nanoparticle using batch technique. The effects different parameters on the sorption processes will be investigated such as contact time and concentration. Kinetics model and sorption isotherm parameters were calculated, and the data showed that the ion exchange of La(III) and Gd(III) on Mn–Ni nanoparticle was spontaneous and endothermic in nature.

*Corresponding author. E-mail: mabdelamid@yahoo.com

EXPERIMENTAL

All reagents and chemicals were of analytical grade purity and used without further purification. pH measurements were performed using pH meter, model 601A, USA. The concentration of La(III) and Gd(III) in solutions was measured by using Shimadzu UV-1800 spectrophotometer. Mn–Ni nanoparticle ion exchange material was prepared by hydrothermal method produces very small particle 18.19 nm as calculated from XRD results using Scherrer formula as described earlier by EL-Aryan [12, 13] as follow, 0.5 M of $MnCL_2$, 0.5 M of $NiCL_2$ and 1.0 M of urea ($CO(NH_2)_2$) were dissolved in 100 mL of deionized water under vigorous a magnetic stirrer at room temperature to form a homogeneous solution. Then, the resulting solution was transferred into a Teflon-lined stainless-steel autoclave (100 mL) to carry out hydrothermal reactions at a certain temperature100 ºC for 24 h to form Mn–Ni nanoparticle. After the autoclave was allowed to cool to the room temperature naturally, the product collected was washed with distilled water and the obtained material was dried in an oven at 60 ºC for 2 days.

Sorption studies

The sorption of La(III) and Gd(III) on Mn–Ni nanoparticle were determined by batch equilibration technique, as a function of different pH values. 0.05 g of Mn–Ni nanoparticle was shaken with 5 mL of 50 mg/L of La(III) and Gd(III) solution at v/m ratio of 100 mL/g. The mixture was placed overnight (sufficient to attain the equilibrium) in a shaker thermostat adjusted at 25, 45 or 65 ± 1 ºC. After equilibrium, the solutions were separated by centrifugation and the concentration of La(III) and Gd(III) in the solution were determined using Shimadzu UV-1800 spectrophotometer. The pH values of the solutions were measured before and after equilibrium using pH meter. The percentage ions adsorption by the ion exchangers was calculated from equation 1:

$$(\%)\ \text{uptake} = (C_i\text{-}C_t)\ /C_i \times 100 \quad (1)$$

where C_i is the initial ion concentration and C_t is the ion concentration in mol L^{-1} at time t.

Kinetics model

The kinetic analysis of the adsorption process for La(III) and Gd(III) on Mn–Ni nanoparticle was carried out by mixing the exchanger with metal ions solution at 50 mg/L with a v/m ratio of 100 mL/g in a shaker thermostat at 25 ± 1 ºC. The kinetic of the adsorption systems were studied using the pseudo-first-order, pseudo-second order, Elovich power model. The intraparticle diffusion model investigated the mechanism of adsorption.

The pseudo first-order kinetic model of Lagergren [14] given by the equation 2:

$$Ln(q_e - q_t) = Ln(q_e) - K_1 t \quad (2)$$

where q_e is the quantity adsorbed at equilibrium (mg/g) and q_t is the quantity absorbed at time t (mg/g). k_1 is the rate constant for the pseudo-first-order sorption (min^{-1}). A linear graph with negative slope is expected from the plot of $\ln(q_e - q_t)$ against t at different concentrations, k_1 and q_{cal} can then be obtained from the slope and intercept respectively. The pseudo-second-order kinetic model [15], presented in equation 3:

$$\frac{t}{q_t} = \frac{1}{K_2 q_e^2} + \frac{t}{q_e} \quad (3)$$

where K_2 is the rate constant of the pseudo-second-order kinetic equation in g/mg min^{-1}, q_e is the maximum sorption capacity in mg/g and q_t (mg/g) is the amount of sorption at time t. Linear graphs are obtained from a plot of t/q_t against t from which q_e and k_2 can be calculated from the

slope and intercepts. The Elovich kinetic model in its linear and nonlinear form is expressed by the equation 4 and 5, respectively [16]:

$$q_t = \frac{1}{\beta} Ln(\alpha\beta) + \frac{1}{\beta} Ln(t) \quad (4)$$

$$q_t = \beta \ln(\alpha\beta t) \quad (5)$$

where q_t is the quantity of adsorbate adsorbed at time t (mg/g), α is a constant related to chemisorption rate and β is a constant which depicts the extent of surface coverage. The two constants (α and β) can be calculated from the intercept and slope of the plot of q_t versus ln t, respectively. The intraparticle diffusion model by Weber and Morris [17] expressed by the mathematical relation in equation 6:

$$q_t = K_3 t^{1/2} + C \quad (6)$$

where qt (mg g^{-1}) is the amount adsorbed at time t and K_3 (mg g^{-1} $min^{-1/2}$) is the rate constant for intraparticle diffusion. Insight into the thickness of the boundary layer can be obtained from the value of C, large intercept suggests great boundary layer effect. A plot of q_t versus $t_{0.5}$ can give a linear or multilinear suggesting that intraparticle diffusion is involved in the adsorption process or two or more steps govern the adsorption process. However, if a linear graph is obtained and the plot passes through the origin then intraparticle diffusion is said to be the sole rate-limiting step [16].

Isothermal studies

The equilibrium of an adsorption process, adsorption isotherm is suitable in describing the distribution of adsorbate molecules between the liquid and the solid phase [18]. Three adsorption isotherms, *viz:* the Langmuir, Freundlich and Temkin models were used to analyze the adsorption data. Important in formation such as adsorption mechanism, favorability of adsorption process and adsorbate-adsorbent affinity may be obtained. The Langmuir isotherm [19] which assumes a surface with homogeneous binding sites, equivalent sorption energies, and no interactions between adsorbed species is expressed by the mathematical relation 7:

$$\frac{C_e}{q_e} = \frac{C_e}{q_{max}} + \frac{1}{q_{max} K_L} \quad (7)$$

where C_e is the equilibrium concentration of ions (mg/L), q_e is the quantity of ions adsorbed onto the adsorbent equilibrium(mg/g), q_{max} is the maximum monolayer adsorption capacity of adsorbent (mg/g) and K_L is the Langmuir adsorption constant(L/mg). The plot of C_e/q_e against C_e gives a straight line with a slope and intercept of $1/q_{max}$ and $1/q_{max}$ K_L respectively. K_L is an important tool in the calculation of the dimensionless equilibrium parameters (R_L) that explains the favorability of adsorption process; R_L is calculated by the mathematical relation in equation 8:

$$RL = \frac{1}{(1 + K_L C_o)} \quad (8)$$

The Freundlich isotherm [20] that is an empirical model not limited to monolayer coverage alone but also describe multi-layer adsorption. It is expressed mathematically as in equation 9:

$$\log q_e = \frac{1}{n} \log C_e + \log K_f \quad (9)$$

where q_e is the quantity of ions adsorbed at equilibrium (mg/g), Ce is the concentration (mg/L) of ions in solution at equilibrium; K_f and n are Freundlich constants incorporating the factors affecting the adsorption capacity and adsorption intensity respectively. The plots of Ln q_e against

Ln C_e gives a linear graph with slope 1/n and intercept log K_f from which n and K_f can be calculated, respectively.

The Temkin isotherm assumes linear rather than logarithm decrease of heat of adsorption while ignoring extremely low and very high concentration. It also assumes uniform distribution of bounding energy up to some maximum bonding energy. It is expressed by equation 10 [21]:

$$q_e = B\ln A + B\ln C_e \quad (10)$$

where q_e is the amount of adsorbate adsorbed at equilibrium (mg/g); C_e is concentration of adsorbate in solution at equilibrium (mg/L). B is a constant related to the heat of adsorption and it is defined by the expression B¼ RT/b, b is the Temkin constant (J/mol), T is the absolute temperature (K), R is the gas constant (8.314 J/mol K), and A is the Temkin isotherm constant (L/g). From the plot of qe vs. $\ln C_e$, B and A can be calculated from the slopes (B) and intercepts (BlnA), respectively [22].

RESULTS AND DISCUSSION

The effect of shaking contact time on La(III) and Gd(III) adsorption onto Mn–Ni nanoparticle was studied using a fixing concentration in the range of (5– 360 min). At the conditions of 25 mg adsorbent, 5 mL volume, pH 5.1, 25 ºC and 100 mg/L of La(III) and Gd(III) as shown in (Figure 1). The uptake increased quickly in the beginning, and then the adsorption equilibrium was obtained after 360 min and 240 min for La(III) and Gd(III), respectively. After that, the adsorption efficiency became constant. Based on these results; the equilibrium time in all adsorption experiments was 360 min and 240 min for La(III) and Gd(III) respectively [23]. In addition, it was observed that the adsorption rates of Gd(III) were very rapid in the initial 60 min, during which 80% of Gd(III) was absorbed, while the adsorption rates of La(III) were slowly in the initial 120 min, during which 23% of La(III) was absorbed onto Mn–Ni nanoparticle ion exchange material, under similar conditions. Also (Figure 1) a and b show the adsorption capacities, q_e increased gradually of La(III) and Gd(III) onto Mn–Ni nanoparticle ion exchange material, respectively. The rapid adsorption may be attributed to the availability of more active sites on the adsorbent surface at the initial stages, and gradual occupancy of these active sites reduced the efficient interactions between metal ions and the adsorbent and adsorption rate became slower [24]. The dissimilarity in adsorption rates between La(III) and Gd(III) can be explained by the adsorption of these ions at different sites on the adsorbent. The adsorption of La(III) is likely due to ion-exchange reactions and electrostatic attraction with negatively charged functional groups on the Mn–Ni nanoparticle ion exchange material, surface that are readily accessible by the adsorbate, resulting in rapid adsorption.

The adsorbate requires a longer time to diffuse through cracks or pores in the alginate-based adsorbent before reaching the active sites. Whereas the subsequent slow step may be due to the competition between metal ions for the remaining available surface sites and the diffusion of metal ions into the inner surface of adsorbent beads [25].

The effect of initial concentration on the adsorption capacity of La(III) and Gd(III) onto Mn–Ni nanoparticle ion exchange material at the optimum pH = 5.1 and at room temperature, the results show that the equilibrium sorption capacities of the Mn–Ni nanoparticle ion exchange material increase with increasing the initial La(III) and Gd(III) concentration. This is because of an increase in the chances of contact between the adsorbent and adsorbed material. Also, because the higher the initial La(III) and Gd(III) concentration, the higher the driving force of the concentration gradient at solid-liquid interface which causes an increase of the amount of La(III) and Gd(III) adsorbed on the adsorbent [24]. When the initial concentration of La(III) and Gd(III) increases from 50 to 400 mg/L, the amount of La(III) and Gd(III) adsorbed onto Mn–Ni nanoparticle ion exchange material at equilibrium (q_e) increases from 4.82 to 9.36 mg/g and from 4.76 to 8.62 mg/g for Mn–Ni nanoparticle, respectively.

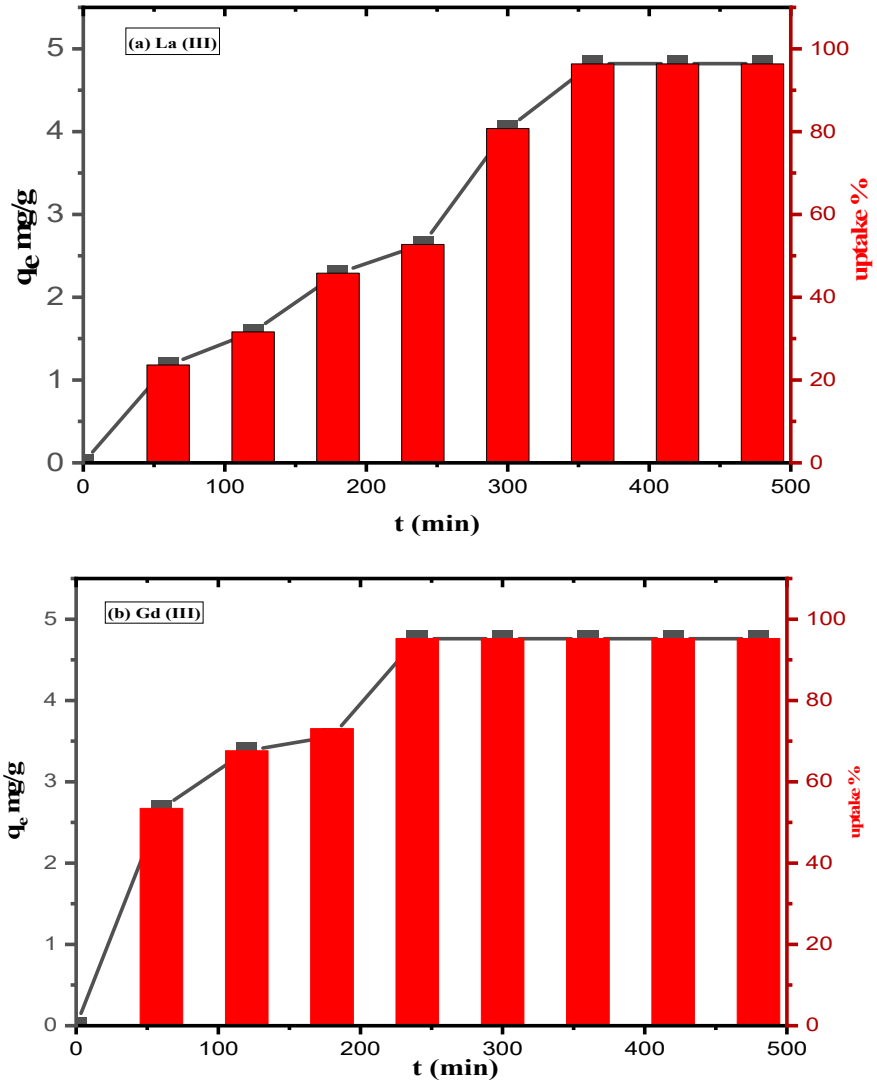

Figure 1. Effect of contact time on the sorption of (a) La(III) and (b) Gd(III) onto Mn–Ni nanoparticle ion exchange material at initial metals concentration of 50 mg/L.

Adsorption kinetics

The parameters of the various kinetics model and the validation results have been reported (Table 1). The pseudo-second order assumes that the rate of adsorption of solute is proportional to the available sites on the adsorbent. The reaction rate is dependent on the amount of solute on the surface of the adsorbent. The pseudo-first-order kinetics fit shows a better linear relationship with high correlation coefficient of $R^2 > 0.973$ for La(III) while the pseudo-second-order kinetics shows

a better linear relationship with high correlation coefficient of $R^2 > 0.91$ for Gd(III) for all experimental conditions as shown in Figure 2 and Table 1. Moreover, calculated values of q_e from the pseudo-second-order kinetics was 6.14 mg/g are in close proximity to experimental results 4.76 mg/g, indicating that adsorption of Gd(III) onto Mn–Ni nanoparticle is in accord with pseudo-second-order kinetics, that is assumed the chemisorption may be the rate-limiting step through sharing or exchange of electrons between the adsorbent and adsorbent [26]. The adsorption of La(III) onto Mn–Ni nanoparticle could be fit also by the pseudo-first-order kinetic model where q_e experimental was 4.818 mg/g is more closed with q_e calculated that was 4.42 mg/g as in Table 1.

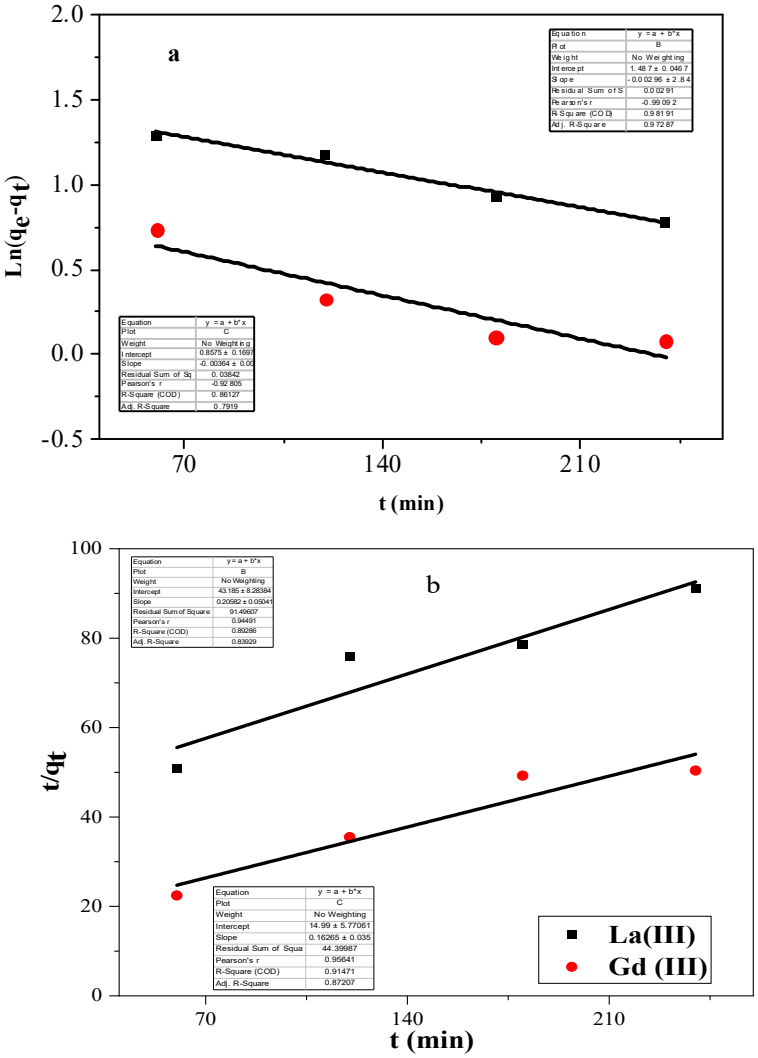

Figure 2. Linearization of the kinetic data through: (a) pseudo first order and (b) pseudo second order for La(III) and Gd(III) adsorption by Mn–Ni nanoparticle ion exchange material.

The intra-particle diffusion model has been widely applied to examine the rate limiting step during adsorption. The adsorption of solute in a solution involves mass transfer of adsorbate (film diffusion), surface diffusion, and pore diffusion. In the intra-particle diffusion if the line of plots of q_t versus t½ passes through the origin, intra-particle diffusion controls the adsorption process. In our study as shown in (Figure 3), the plots of q_t versus t½, involved two linear steps take place with correlation coefficients ($R^2 > 0.97$). The sharper first stage portion (a) is attributed to the diffusion of adsorbate though the solution to the external surface of adsorbent or the boundary layer diffusion of solute molecules. The second portion (b) describes the gradual adsorption stage until equilibrium is reached. During these two stages, La(III) and Gd(III) are slowly transported via intra-particle diffusion in the particles of Mn–Ni nanoparticle and are finally retained in the pores. The slope of the line of the first stage is called the intra-particle linear portion of the first stage does not pass though the origin, indicating there is a boundary layer resistance between adsorbent and adsorbate and There are different mechanisms that control the adsorption process [27].

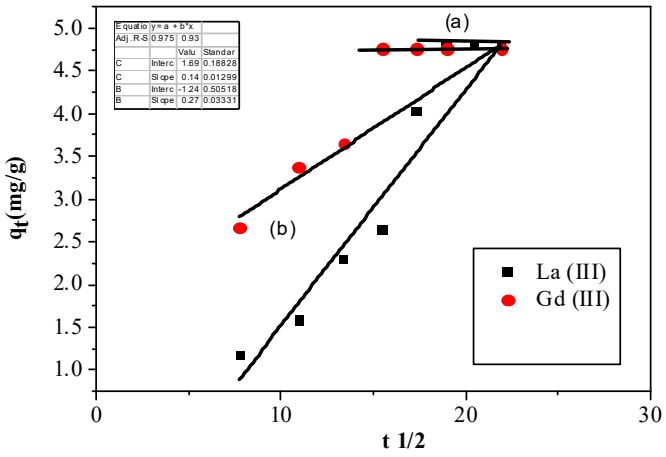

Figure 3. Linearization of the intra-particle diffusion portion (a) and portion (b) for La(III) and Gd(III) adsorption by Mn–Ni nanoparticle ion exchange material.

There are four main mechanisms that describe the transfer of solute from a solution to the adsorbent. The first is called mass transfer (bulk movement) of solute particles as soon as the adsorbent is dropped into the solution. This process is too fast; thus, it is not considered during the design of kinetic systems. The second mechanism is called film diffusion; it involves the slow movement of solutes from the boundary layer to the adsorbent's surface. When the solute reaches the surface of the adsorbent, they move to the pores of the adsorbent third mechanism. The final mechanism involves rapid adsorptive attachment of the solute on the active sites of the pores; being a rapid process [27]. In general, it is observed that values of K_3 of Gd(III) is more than the values of La(III) of the adsorption on Mn–Ni nanoparticle ion exchange material.

The Elovich kinetic model is useful in describing adsorption on highly heterogeneous adsorbents with a fast rate and helps to predict the mass and surface diffusion, activation, and deactivation energy. The constants α and β can be obtained from the slope and intercept of the plot of q_t vs ln t and are show in (Figure 4) and listed in Table 1. In the case of using the Elovich equation, the correlation coefficients (R^2) are obtained in the range of 0.99 for La(III) and 0.85 for Gd(III) onto Mn–Ni nanoparticle, respectively.

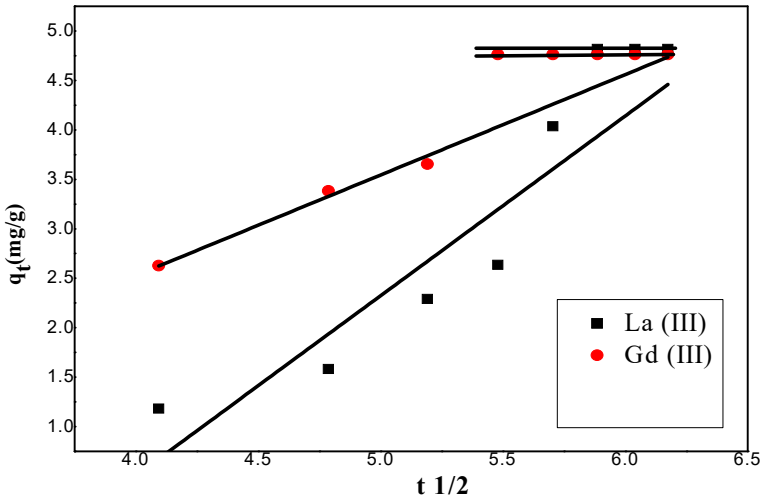

Figure 4. Linearization of the Elovich for La(III) and Gd(III) adsorption by Mn–Ni nanoparticle ion exchange material.

Table 1. Kinetic parameters for La(III) and Gd(III) adsorption by Mn–Ni nanoparticle ion exchange material.

Parameters	Mn–Ni nanoparticle	
Pseudo-first order	La(III)	Gd(III)
q_e (mg/g) (calculated)	4.42	2.36
q_e (mg/g) (experiment)	4.81	4.76
K_1 (min^{-1})	0.00295	0.00364
R^2	0.973	0.792
Pseudo-second order		
q_e (mg/g) (calculated)	4.88	6.14
q_e (mg/g) (experiment)	4.81	4.763
K_2 (g/mg min)	0.00097	0.00177
R^2	0. 89	0.91
Intraparticle diffusion		
K_3 (mg/g $min^{1/2}$)	0.1491	0.2761
C (mg/g)	1.697	-1.2409
R^2	0.975	0.931
Elovich kinetic model		
α (mg/g min)	0.224	0.044
β(g/mg)	0.984	0.550
R^2	0.993	0.854

Adsorption isotherms

The values of q_{max} and K_L were determined by plotting C_e/q_e versus C_e (Figure 5) and their values are given in Table 3. It was noted that the vales of correlation coefficient R^2 was 0.995 for adsorption of La(III) onto Mn–Ni nanoparticle R^2 was 0.991 for adsorption of Gd(III) onto Mn–Ni nanoparticle. The vales of the maximum adsorption capacity from the Langmuir model q_{max} values were 8.81 and 7.77 mg/g for adsorption of La(III) and Gd(III) onto Mn–Ni nanoparticle. R_L value indicates any one of the four possible adsorption characteristics: $R_L > 1$ for

unfavorable adsorption; $R_L = 0$ for irreversible sorption. The dimensionless constants R_L obtained from the Langmuir model were $R_L < 1$ for adsorption La(III) indicating favorable adsorption and $R_L > 1$ for Gd(III) unfavorable adsorption. Table 2 reports the various parameters obtained from Langmuir model.

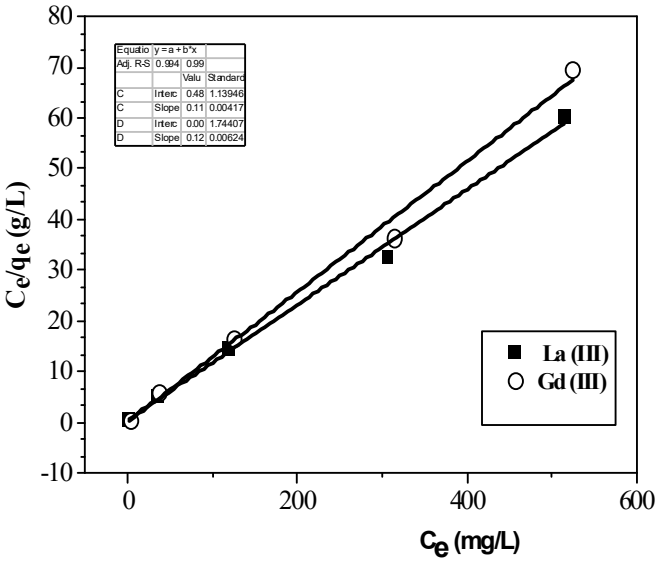

Figure 5. Langmuir isotherm plots for La(III) and Gd(III) adsorption by Mn–Ni nanoparticle.

The Plots of Ln q_e against Ln C_e gives a linear graph with slope 1/n and intercept Ln K_f from which n and K_f can be calculated, respectively. 1/n is related to the intensity of the adsorption. Freundlich adsorption isotherm constants K_F and n were determined from the intercept and slope of a plot of Ln q_e versus Ln Ce (Figure 6). Table 2 reports the various parameters obtained from the Freundlich isotherm plots. Isotherms with $1/n < 1$ indicate the high affinity between both adsorbate and adsorbent and imply the presence of chemisorption reaction. The values of 1/n obtained in this study were observed to be less than unity which indicates favorable adsorption. The vales of correlation coefficient R^2 was 0.931 and 0.872for adsorption of La(III) and Gd(III) onto Mn–Ni nanoparticle, respectively. The data were fitted with Langmuir model better than Freundlich model indicating homogeneous adsorption should have occurred on the surface of Mn–Ni nanoparticle [28].

The Temkin isotherm model considers the interactions between adsorbent and metal ions and is based on the assumption that the free energy of adsorption is a function of the surface coverage [29]. Temkin model shows in (Figure 7) was used for the further analysis. And different from the Langmuir and Freundlich models, Temkin model assumes that adsorption energy decreases linearly with the surface coverage and is more applicable to chemical adsorption process [23]. The actual experimental data complied with the Temkin model in a relatively small coverage range, where chemical adsorption took place. Therefore, the obtained comparatively weak linear correlation coefficients were 0.894 and 0.828 of La(III) and Gd(III) onto Mn–Ni nanoparticle, respectively, was fit with the Temkin model manifested that the chemical adsorption was not the only dominated interaction for La(III) and Gd(III) onto Mn–Ni nanoparticle.

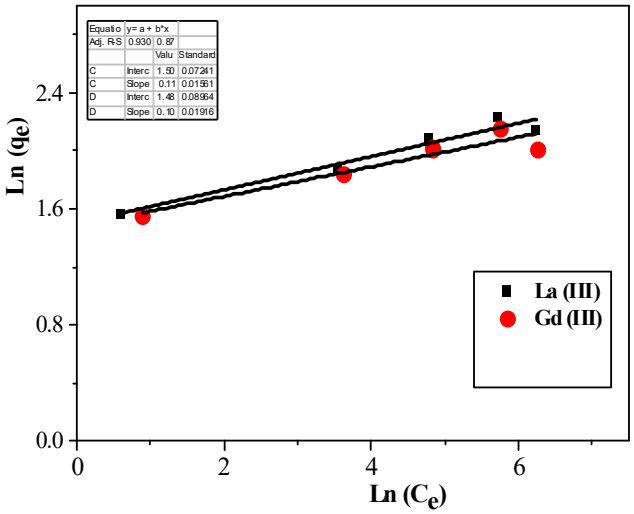

Figure 6. Freundlich isotherm plots for La(III) and Gd(III) adsorption by Mn–Ni nanoparticle.

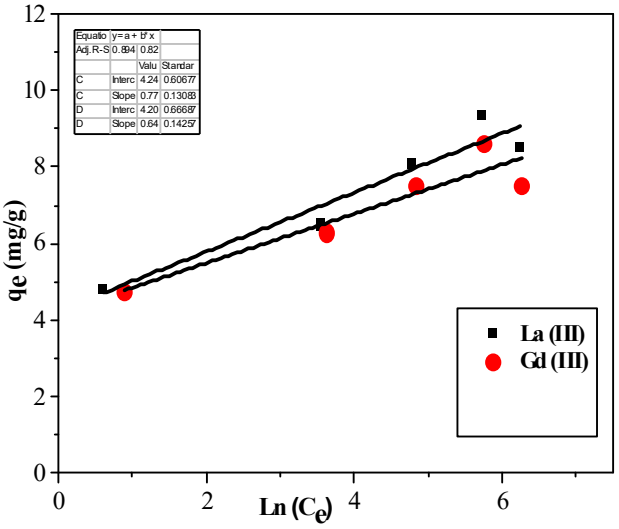

Figure 7. Temkin isotherm plots for La(III) and Gd(III) adsorption by Mn–Ni nanoparticle.

Table 2. Summarized Langmuir, Freundlich and Temkin isotherm parameters for La(III) and Gd(III) adsorption by Mn–Ni nanoparticle.

	Mn–Ni nanoparticle	
Langmuir isotherm parameters	La(III)	Gd(III)
q_{max} (mg/g)	8.81	7.77
K_L (L/mg)	0.233	13.71
R^2	0.995	0.991
Freundlich isotherm parameters		
1/n	0.1155	0.1011
K_F ($mg^{n-1}/g.L^n$)	4.49	4.41
R^2	0.931	0.872
Temkin isotherm parameters		
A_T(L/mg)	241.29	689.5
b_T	3205	3853
R^2	0.894	0.828

Table 3. A comparison of the isotherm parameters for La(III) and Gd(III) adsorption onto various adsorbents.

Adsorbent material	Sorption capacity (mg g^{-1})		References
	La(III)	Gd(III)	
Aliquat-336 impregnated onto Amberlite XAD-4	4.73	4.44	[30]
Nanoporous aluminosilicates	1.25	-	[31]
Neem sawdust	2.3	-	[32]
Bis-picolyamine resin (M4195)	9.85	-	[33]
Prawn carapace	7.9	-	[32]
Zirconium triethylenetetramine (ZrT)	6.07	-	[34]
Mn–Ni nanoparticle	8.81	7.77	This work

CONCLUSION

The prepared Mn–Ni nanoparticle has highly efficient adsorption of La(III) than Gd(III) from aqueous solution. The maximum adsorption percentage for La(III) and Gd(III) attained at pH 5.1. The adsorption efficiency of La(III) and Gd(III) was 96.36 and 95.13, respectively. The equilibrium time for adsorption of La(III) and Gd(III) was attained at 240 min and 180 min, respectively. The adsorption capacities for La(III) and Gd(III) was 9.36 and 8.62 mg/g, respectively. The adsorption capacity of Mn–Ni nanoparticle was highly dependent on the initial La(III) and Gd(III) concentrations. The sorption of the studied La(III) and Gd(III) from aqueous suspension using the Mn–Ni nanoparticle was fitted well to Langmuir and pseudo second order equations. Thus, the Mn–Ni nanoparticle could be excellent adsorbent for adsorption of La(III) and Gd(III) from aqueous solutions comparing with other adsorbents.

ACKNOWLEDGMENTS

The authors are thankful to the Deanship of Scientific Research at University of Bisha for supporting this work through the Fast-Track Research Support Program.

REFERENCES

1. Moldoveanu, G.A.; Papangelakis, V.G. An overview of rare-earth recovery by ion-exchange leaching from ion-adsorption clays of various origins. *Mineral. Mag.* **2016**, 80, 63–76.

2. Nabi, S.A.; Naushad, M. Studies of cation-exchange thermodynamics for alkaline earths and transition metal ions on a new crystalline cation-exchanger aluminium tungstate: Effect of the surfactant's concentration on distribution coefficients of metal ions. *Colloids Surfaces A Physicochem. Eng. Asp.* **2007**, 293, 175–184.
3. Nabi, S.A.; Naushad, M.; Khan, A.M. Sorption studies of metal ions on napthol blue–black modified Amberlite IR-400 anion exchange resin: Separation and determination of metal ion contents of pharmaceutical preparation. *Colloids Surfaces A Physicochem. Eng. Asp.* **2006**, 280, 66–70.
4. Nabi, S.A.; Ganai, S.A.; Naushad, M. Preparation and characterization of a new inorganic cation-exchanger: Zirconium(IV) iodosilicate: Analytical applications for metal content determination in pharmaceutical sample and synthetic mixture. *Desalin. Water Treat.* **2010**, 16, 29–38.
5. AL-Othman, Z.A.; Inamuddin; Naushad, M. Forward (M^{2+}–H^{+}) and reverse (H^{+}–M^{2+}) ion exchange kinetics of the heavy metals on polyaniline Ce(IV) molybdate: A simple practical approach for the determination of regeneration and separation capability of ion exchanger. *Chem. Eng. J.* **2011**, 171, 456–463.
6. AL-Othman, Z.A.; Naushad, M.; Inamuddin. Organic–inorganic type composite cation exchanger poly-*o*-toluidine Zr(IV) tungstate: Preparation, physicochemical characterization and its analytical application in separation of heavy metals. *Chem. Eng. J.* **2011**, 172, 369–375.
7. ALOthman, Z.A.; Naushad, M.; Ali, R. Kinetic, equilibrium isotherm and thermodynamic studies of Cr(VI) adsorption onto low-cost adsorbent developed from peanut shell activated with phosphoric acid. *Environ. Sci. Pollut. Res.* **2013**, 20, 3351–3365.
8. Zhou, J.; Duan, W.; Zhou, X.; Zhang, C. Application of annular centrifugal contactors in the extraction flowsheet for producing high purity yttrium. *Hydrometallurgy* **2007**, 85, 154–162.
9. Saleh, T.A.; Gupta, V.K. *An Overview of Membrane Science and Technology* in *Nanomaterial and Polymer Membranes*, Elsevier: Online Publication; **2016**; pp. 1–23.
10. Dewulf, B.; Riaño, S.; Binnemans, K. Separation of heavy rare-earth elements by non-aqueous solvent extraction: Flowsheet development and mixer-settler tests. *Sep. Purif. Technol.* **2022**, 290, 120882.
11. Fang, H.; Cole, B.E.; Qiao, Y.; Bogart, J.A.; Cheisson, T.; Manor, B.C. Electro-kinetic separation of rare earth elements using a redox-active ligand. *Angew. Chemie* **2017**, 129, 13635–13639.
12. El-Aryan, Y.F.; Alqahtany, F.Z.; Melhi, S. Manganese vanadate and polymethylmethacrylate based ion exchange materials: Synthesis, characterization, and selectivity in the sorption of Eu and Co radionuclides. *Russ. J. Phys. Chem. A* **2020**, 94, 1319–1329.
13. Khalil, M.; El-Aryan, Y.F.; Ali, I.M. Hydrothermal synthesis of Mn–Fe nano oxides and their composite for removal of Zn^{2+}, Ni^{2+} and Co^{2+} from simulated radioactive waste. *J. Inorg. Organomet. Polym. Mater.* **2016**, 26, 359–369.
14. Lagergren, S.; Svenska, B.S. On the theory of so-alled dsorption of materials. *R. Swed. Acad. Sci. Doc. Band.* **1898**, 24, 1–13.
15. Ho, Y.; McKay, G. Pseudo-second order model for sorption processes. *Process. Biochem.* **1999**, 34, 451–465.
16. Avrami, M. Kinetics of phase change. II Transformation-time relations for random distribution of nuclei. *J. Chem. Phys.* **1940**, 8, 212–224.
17. Weber, W.J.; Morris, J.C. Kinetics of adsorption on carbon from solution. *J. Sani. Eng. Div.* **1963**, 89, 31–59.
18. Kyzas, G.Z.; Matis, K.A. Nanoadsorbents for pollutants removal: A review. *J. Mol. Liq.* **2015**, 203, 159–168.
19. Langmuir, I. The constitution and fundamental properties of solids and liquids. Part I. Solids. *J. Am. Chem. Soc.* **1916**, 38, 2221–2295.

20. Freundlich, H. Über die adsorption in lösungen. *Zeitschrift für Phys. Chemie* **1907**, 57, 385–470.
21. Temkin, M.I.; Pyzhev, V. Kinetics of ammonia synthesis on promoted iron catalysts. *Acta Physiochim.* **1940**, 12, 327–356.
22. Inyinbor, A.A.; Adekola, F.A.; Olatunji, G.A. Kinetics, isotherms and thermodynamic modeling of liquid phase adsorption of Rhodamine B dye onto *Raphia hookerie* fruit epicarp. *Water Resour. Ind.* **2016**, 15, 14–27.
23. Khalil, M.; Shehata, M.M.; Ghazy, O.; Waly, S.A.; Ali, Z.I. Synthesis, characterization and γ-rays irradiation of cobalt-based metal-organic framework for adsorption of Ce(III) and Eu(III) from aqueous solution. *Radiat. Phys. Chem.* **2022**, 190, 109811.
24. Abdel-Galil, E.A.; Ibrahim, A.B.; Abou-Mesalam, M.M. Sorption behavior of some lanthanides on polyacrylamide stannic molybdophosphate as organic–inorganic composite. *Int. J. Ind. Chem.* **2016**, 7, 231–240.
25. El-Aryan, Y.F.; Alqahtany, F.Z. Removal of some heavy metals from wastewater using hydrothermally synthesized zirconium phosphate as ion exchange material. *Russ. J. Phys. Chem. A* **2021**, 95, 209–216.
26. Ahmad, M.A.; Ahmad, N.; Bello, O.S. Removal of remazol brilliant blue reactive dye from aqueous solutions using watermelon rinds as adsorbent. *J. Dispers. Sci. Technol.* **2015**, 36, 845–858.
27. Liu, X.; Demir, N.K.; Wu, Z.; Li, K. Highly water-stable zirconium metal–organic framework UiO-66 membranes supported on alumina hollow fibers for desalination. *J. Am. Chem. Soc.* **2015**, 137, 6999–7002.
28. Khalil, M.; El-Aryan, Y.F.; El Afifi, E.M. Sorption performance of light rare earth elements using zirconium titanate and polyacrylonitrile zirconium titanate ion exchangers. *Part. Sci Technol.* **2018**, 36, 618–627.
29. Hayes, E.K.; Stoddart, A.K.; Gagnon, G.A. Adsorption of SARS-CoV-2 onto granular activated carbon (GAC) in wastewater: Implications for improvements in passive sampling. *Sci. Total Environ.* **2022**, 847, 157548.
30. Elsofany, E. Removal of lanthanum and gadolinium from nitrate medium using Aliquat-336 impregnated onto Amberlite XAD-4. *J. Hazard. Mater.* **2008**, 153, 948–954.
31. Sepehrian, H.; Cheraghali, R.; Rezaei, P.; Abdi, H.A. Adsorption behavior of lanthanum on modified nanoporous aluminosilicates. *Int. J. Ind. Chem.* **2011**, 2, 235–241.
32. Sre, J.; Varshini, C.J.; Das, N. Relevant approach to assess the performance of biowaste materials for the recovery of lanthanum(III) from aqueous medium. *Res. J. Pharm. Biol. Chem. Sci.* **2014**, 5, 88–94.
33. Botelho, Junior, A.B.; Pinheiro, É.F.; Espinosa, D.C.R.; Tenório, J.A.S.; Baltazar, M.; dos, P.G. Adsorption of lanthanum and cerium on chelating ion exchange resins: Kinetic and thermodynamic studies. *Sep. Sci. Technol.* **2022**, 57, 60–69.
34. Lankapati, H.M.; Dankhara, P.M.; Lathiya, D.R.; Shah, B.; Chudasama, U.V.; Choudhary, L. Removal of lanthanum, cerium and thorium metal ions from aqueous solution using ZrT hybrid ion exchanger. *Sustain. Energy Technol. Assess.* **2021**, 47, 101415.